ACS Catalysis

Research Article

pubs.acs.org/acscatalysis

Cocatalytic Effect of $SrTiO_3$ on Ag_3PO_4 toward Enhanced Photocatalytic Water Oxidation

Xiangjiu Guan and Liejin Guo*

International Research Center for Renewable Energy, and State Key Laboratory of Multiphase Flow in Power Engineering, Xi'an Jiaotong University, Xi'an 710049, China

Supporting Information

ABSTRACT: Ag_3PO_4 has been reported to be an excellent photocatalyst for O_2 evolution from aqueous solution, which makes it a promising candidate for designing a Z-scheme water-splitting system. In this work, in order to further improve the photocatalytic activity, a series of $SrTiO_3/Ag_3PO_4$ composite photocatalysts was constructed by introducing $SrTiO_3$ (with a less positive valence band minimum) to Ag_3PO_4 and was synthesized by two consecutive hydrothermal processes. The obtained photocatalysts were systematically characterized by XRD, SEM, BET, UV−vis, etc., showing that $SrTiO_3/Ag_3PO_4$ composites were formed by coating $SrTiO_3$ onto a Ag_3PO_4 polyhedron. Photocatalytic O_2 evolution results demonstrated that a small amount of $SrTiO_3$ brought about significant enhancement of photocatalytic activity of Ag_3PO_4 and that the apparent quantum yield at 420 nm reached 16.2% with a molar ratio of $SrTiO_3$ to Ag_3PO_4 equal to 1/20, which led to the fact that $SrTiO_3$ could serve as cocatalyst for water oxidation providing both accelerated electron−hole separation by band gap alignment and more active sites by enlarged surface area.

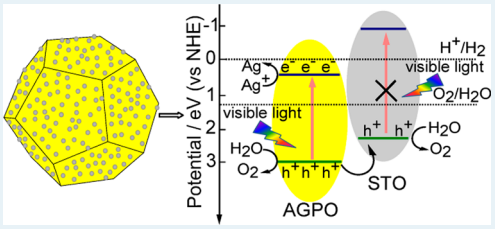

KEYWORDS: *$SrTiO_3$, Ag_3PO_4, cocatalysis, photocatalysis, O_2 evolution*

1. INTRODUCTION

Photocatalytic water splitting assisted by a semiconductor has been considered to be one of the most promising approaches for solving both energy and environmental issues worldwide.[1−4] Water splitting can be separated to two half reactions, namely, hydrogen production and oxygen production.[5−7] As hydrogen production has been quite efficiently achieved during the past decade, fabrication of a robust photocatalyst for oxygen evolution still remains a challenge due to the more complicated four electron process.[8−14] Recently, Ag_3PO_4 has been reported to be an excellent photocatalyst for water oxidation and thus drew tremendous attention.[15] Because of its highly dispersive conduction-band structure resulting from delocalized *d* states, a small effective mass of electron was obtained, which facilitated the immigration of photoexcited electrons and holes.[16] Tetrahedral Ag_3PO_4 composed of {111} facets was synthesized by Martin et al. through a kinetic control method, and it performed greater activity in water photooxidation than those composed of {100} and {110} faceted crystals.[17] In our previous work, enhanced O_2 evolution activity was also achieved from the better crystallization and more regulated morphology by virtue of hydrothermal treatment, followed by optimization of reaction conditions such as temperature, pH, etc. for hydrothermal preparation of Ag_3PO_4.[18]

It is widely accepted that coupling semiconductor materials with matched band-edges could facilitate the immigration and separation of photogenerated electrons and holes, and indeed benefit the photocatalytic activity and stability.[19] Some composites of Ag_3PO_4 ($CQDs/Ag_3PO_4$,[20] Ag_3PO_4/TiO_2,[21] Ag_3PO_4/graphene(oxide),[22−27] $Ag_3PO_4/CNTs$,[28] and g-C_3N_4/Ag_3PO_4[29]) were also reported to give better activity for eliminating organic pollutants. As for O_2 evolution, few heterostructured photocatalysts based on Ag_3PO_4 were evaluated.[30] $SrTiO_3$ is a stable semiconductor that has been widely studied as photocatalyst for water splitting,[31−35] whose minimum conduction band (CBM) and maximum valence band (VBM) are both negative compared to those of Ag_3PO_4. Guo et al. designed a heterojunction of Ag_3PO_4 and Cr-$SrTiO_3$, and proved the accelerated electron and hole transportation between them.[36] The designed heterojunction showed superior performance in IPA photodegradation than separated materials. However, low activity for O_2 evolution was obtained.

In this contribution, pure phase $SrTiO_3$ was introduced to Ag_3PO_4, in order to further enhance the photo oxidation activity of Ag_3PO_4 by providing a cocatalytic effect. Several unique advantages of pure phase $SrTiO_3$ were taken into consideration. First, efficient charge separation could be achieved between $SrTiO_3$ and Ag_3PO_4 due to their matched band-edges. Second, differing from the traditional noble metal cocatalyst, loading pure $SrTiO_3$ avoided obstructing visible light absorption of Ag_3PO_4. Third, unlike Cr-$SrTiO_3$, pure $SrTiO_3$ was not excited under visible-light irradiation, which protected Ag_3PO_4 from being reduced by photogenerated electrons of $SrTiO_3$ and facilitated the concentrating of research on the cocatalytic effect of $SrTiO_3$. A series of $SrTiO_3/Ag_3PO_4$ photocatalysts was synthesized by a two-consecutive hydro-

Received: April 17, 2014
Revised: July 29, 2014
Published: July 29, 2014

   dx.doi.org/10.1021/cs5005079 | ACS Catal. 2014, 4, 3020−3026

thermal process. The properties of photocatalysts such as crystal structure, optical property, morphology, and photocatalytic activity were systematically characterized and evaluated, and the mechanism of the improved photocatalytic activity of $SrTiO_3/Ag_3PO_4$ composite was proposed.

2. EXPERIMENTAL SECTION

2.1. Materials and Sample Preparation. All of the reagents were purchased from Sinopharm Reagent Company, China and used without further purification.

2.1.1. Synthesis of Pure Phase $SrTiO_3$. Pure phase $SrTiO_3$, with a particle size of 20−50 nm, was synthesized by a hydrothermal method. In a typical synthesis, 10 mmol $Ti(C_4H_9O)_4$ was dissolved in 20 mL of ethylene glycol (EG) to form a clear solution, to which 20 mL of 0.5 M $Sr(NO_3)_2$ aqueous solution was then dropped in, and 10 mL of 5 M NaOH was finally added. After stirring for 30 min, the mixture was transferred into a Teflon-lined stainless autoclave and then heated at 200 °C for 24 h. The obtained products were washed with water and ethanol until the pH reached 7 and then dried overnight at 70 °C.

2.1.2. Synthesis of $SrTiO_3/Ag_3PO_4$ Composite. The $SrTiO_3/Ag_3PO_4$ composite was synthesized following the hydrothermal treatment procedure according to our previous report.[18] In a typical synthesis, 45.87 mg of $SrTiO_3$ was dispersed into 40 mL of distilled water and ultrasonically treated for 10 min. After that, 15 mmol $AgNO_3$ was quickly added and dissolved by stirring. Then, 40 mL of 0.125 M Na_3PO_4 solution was dropped in, and a yellow precipitate appeared immediately. The obtained mixture were transferred into a Teflon-lined stainless autoclave and then heated at 100 °C for 24 h, followed by washing the product with distilled water three times and drying at 70 °C for 6 h. The collected product was designated as SA-1/20.

$SrTiO_3/Ag_3PO_4$ composites with different molar ratios (1/50, 1/20, 1/10, 1/5, 1/2, and 1/1) were obtained by simply adjusting the usage of $SrTiO_3$ and were designated as SA-*x*, in which *x* refers to the molar ratio of $SrTiO_3$ and Ag_3PO_4.

2.2. Characterization. X-ray diffraction (XRD) patterns were identified by a PANalytical X'pert MPD Pro diffractometer using Ni-filtered Cu Kα irradiation (λ = 1.5406 Å, 40 kV, 40 mA) and a scan rate of 2°/ min in the 2θ range from 10° to 80°. UV−vis absorption spectra of the samples were recorded with a Hitachi U-4100 UV−vis-near-IR spectrophotometer using $BaSO_4$ as reference. FESEM images and energy dispersive spectra (EDS) of the samples were observed by JEOL JSM-7800F field emitting scanning electron microscope. The surface area measurement was carried out by the N_2 adsorption isotherms conducted in the Micromeritics ASAP 2020 plus instrument using the Brunauer−Emmette−Teller (BET) method. X-ray photoelectron spectroscopy (XPS) data were collected from a Kratos Axis-Ultra DLD instrument with a monochromatized Al Kα line source (150 W), and all binding energies were referenced to the C 1s peak at 284.8 eV. Photoluminescence (PL) emission spectra were obtained on a PTI QM-4 fluorescence spectrophotometer at room temperature using an excitation wavelength of 325 nm.

2.3. Evaluation of Photocatalytic Activity. The photocatalytic activity for O_2 evolution under visible-light irradiation was performed in a Pyrex glass cell with a side window. A 300 W Xe arc lamp with a UV cutoff filter (λ > 420 nm) was used as light source. Photocatalyst (0.2 g) was dispersed into 180 mL of 0.02 M $AgNO_3$ solution, in which $AgNO_3$ acted as the sacrificial reagent. After purging with nitrogen gas to eliminate air, the dispersion was irradiated under light with a constant stirring velocity and at a constant temperature around 35 °C kept by thermostatic circulating water. The evolved O_2 was analyzed by a chromatography (Ar as carrier gas) with a NaX zeolite column and an online thermal conductivity detector (TCD).

Apparent quantum yield (A.Q.Y.) was measured using a 420 nm band-pass filter and an irradiate-meter, and calculated according to the following equation:

$$\text{A.Q.Y}\ (\%) = \frac{\text{the number of reacted electrons}}{\text{the number of incident photons}} \times 100 = \frac{\text{the number of evolved } O_2 \text{ molecules} \times 4}{\text{the number of incident photons}} \times 100$$

The turnover number (T.O.N.) in terms of silver ions in the photocatalysts was calculated according to the following equation:

$$\text{T.O.N.} = \frac{\text{the number of reacted electrons}}{\text{the number of silver ions in the photocatalyst}}$$

3. RESULTS AND DISCUSSION

3.1. Characterization of As-Prepared Samples. Composition and crystallographic structure of the as-prepared $SrTiO_3/Ag_3PO_4$ photocatalysts were determined by XRD and are depicted in Figure 1. For comparison, pure $SrTiO_3$ was also included. As shown in Figure 1, all of the diffraction peaks of Ag_3PO_4 were well matched with the body-centered cubic structure of Ag_3PO_4 (JCPDS No. 01-084-0510; space group, $P\bar{4}3n$; a = 6.0110 Å), while those of $SrTiO_3$ corresponded to cubic phase $SrTiO_3$ (JCPDS No. 01-079-0176; space group, Pm-3m; a = 3.9046 Å). XRD patterns of $SrTiO_3/Ag_3PO_4$ composites showed a combination of $SrTiO_3$ and Ag_3PO_4, and rule out the possibility of other impurity phases, indicating successful synthesis of composites. Hydrothermal treatment gave well-crystallized Ag_3PO_4 powder with sharp diffraction peaks. Compared to Ag_3PO_4, peaks of $SrTiO_3$ were broader and less sharper, which may be resulting from the smaller

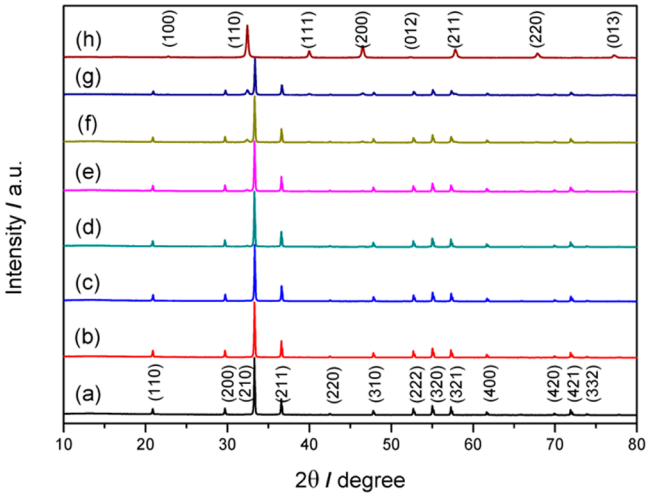

Figure 1. XRD pattern of $SrTiO_3/Ag_3PO_4$ composites with different molar ratios: (a) Ag_3PO_4, (b) SA-1/50, (c) SA-1/20, (d) SA-1/10, (e) SA-1/5, (f) SA-1/2, (g) SA-1/1, and (h) $SrTiO_3$.

dx.doi.org/10.1021/cs5005079 | ACS Catal. 2014, 4, 3020−3026

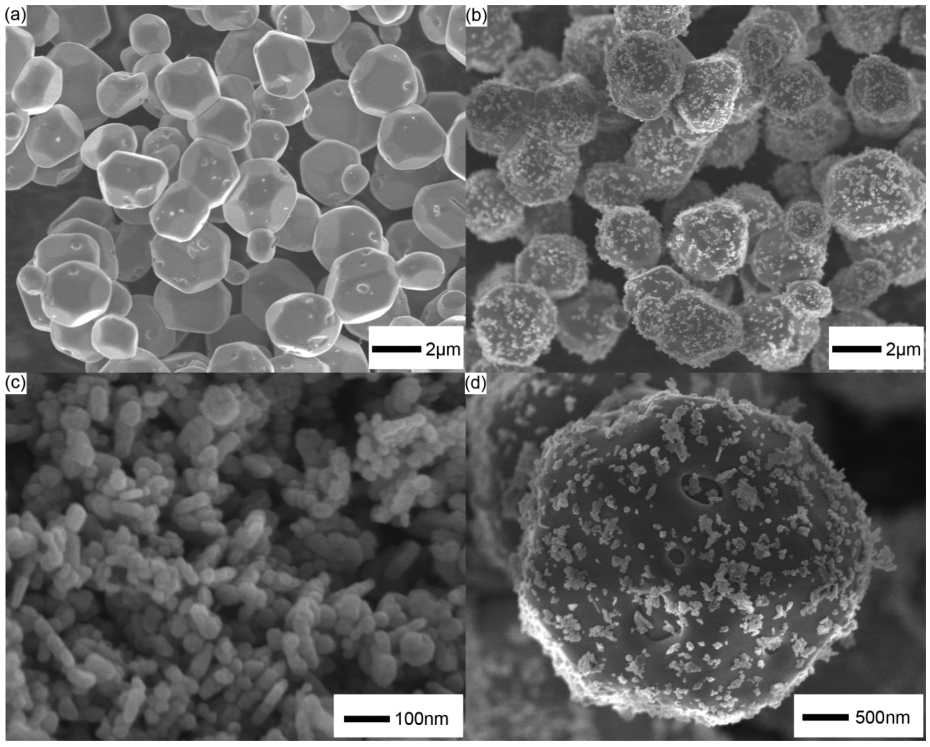

Figure 2. FESEM images of (a) Ag_3PO_4, (b) SA-1/20, (c) $SrTiO_3$, and (d) SA-1/20 in high magnification.

Table 1. BET Surface Area of $SrTiO_3/Ag_3PO_4$ Composites

sample	Ag_3PO_4	SA-1/50	SA-1/20	SA-1/10	SA-1/5	SA-1/2	SA-1/1	$SrTiO_3$
surface area ($m^2\ g^{-1}$)	0.43	1.02	1.74	1.89	2.12	5.21	8.15	27.96

crystal size.[37] Moreover, as the molar ratio of $SrTiO_3$ and Ag_3PO_4 increased from 0 to 1/1, peaks of $SrTiO_3$ became stronger, and the intensity ratio of (110) peaks in $SrTiO_3$ to (210) peaks in Ag_3PO_4 also increased in the XRD pattern of $SrTiO_3/Ag_3PO_4$ composites.[38]

FESEM was used to investigate the morphology and particle size of as-prepared samples. Typical FESEM images of $SrTiO_3$, Ag_3PO_4, and $SrTiO_3/Ag_3PO_4$ composites are presented in Figure 2. Pure $SrTiO_3$ were spherical particles with diameters in the range of 20−50 nm, while Ag_3PO_4 possessed polyhedral morphology at the size of several micrometers with a smooth surface. As for $SrTiO_3/Ag_3PO_4$ composites, it could be clearly seen that $SrTiO_3$ particles were uniformly and tightly attached on the facet of Ag_3PO_4, which indicated an intimate contact between $SrTiO_3$ and Ag_3PO_4.[39] As can be seen from Figure S1 (Supporting Information), a low molar ratio of $SrTiO_3/Ag_3PO_4$ led to good dispersion of $SrTiO_3$ onto the facet of Ag_3PO_4, and assembling of $SrTiO_3$ occurred as the molar ratio increased, which reduced the effective area of contact between two materials.

The surface area of $SrTiO_3/Ag_3PO_4$ composites was measured and listed in Table 1. BET surface area of as-synthesized $SrTiO_3$ particles was 27.96 $m^2\ g^{-1}$, which was much larger than that of Ag_3PO_4 due to its small particle size. Therefore, with $SrTiO_3$ content increasing, the surface area of the $SrTiO_3/Ag_3PO_4$ composite was remarkably enlarged compared to that of pure Ag_3PO_4. Typically, the BET surface area of $SrTiO_3/Ag_3PO_4$ (1/20) composite was 4-fold that of pure Ag_3PO_4.[40−43]

To investigate the elemental composition and chemical states of the as-prepared samples, XPS measurement was carried out, and the results are depicted in Figure 3. In Figure 3a, the two peaks in the spectra of Ag_3PO_4 appearing at 373.85 and 367.85 eV could be ascribed to the binding energies of Ag 3d3/2 and Ag 3d5/2. Peaks located in the same position were also found in the spectra of $SrTiO_3/Ag_3PO_4$, accompanied by peaks at 375.32 and 369.32 eV. The bands at 373.85 and 367.85 eV were attributed to Ag^+, and those at 375.32 and 369.32 eV were attributed to Ag^0 species.[44] This result indicated the appearance of metallic Ag in $SrTiO_3/Ag_3PO_4$. Considering that neither the diffraction peaks in XRD nor the clues of Ag in FESEM images were observed, the detected metallic Ag should be tiny and well dispersed in the $SrTiO_3/Ag_3PO_4$ composite.[41] The molar ratio of metallic Ag to Ag_3PO_4 in SA-1/20 calculated from Figure 3b amounted to be 3/10. It has to be noted that this value was overestimated because XPS signals were mainly collected from the surface of the sample with depth less than 10 nm. XPS etching with Ar^+ on SA-1/20 was then carried out, and signals of metallic Ag disappeared after etching for 20 s. Another calculation based on the EDS result showed that the molar ratio of Ag to Ag_3PO_4 was 3.2%. XPS and EDS results confirmed that the metallic Ag was dispersed on the surface of Ag_3PO_4 (see Figure S12, Figure S13, and Table S1 in Supporting Information). As mentioned in the Experimental Section, Ag_3PO_4 precipitated rapidly when the $Na_2(PO_4)_3$ solution was added to the Ag^+ solution containing suspended $SrTiO_3$. It could be deduced that a trace amount of Ag^+ on the surface of Ag_3PO_4 was reduced by organic residuals adsorbed on $SrTiO_3$ during the high temperature and high pressure hydrothermal

dx.doi.org/10.1021/cs5005079 | ACS Catal. 2014, 4, 3020−3026

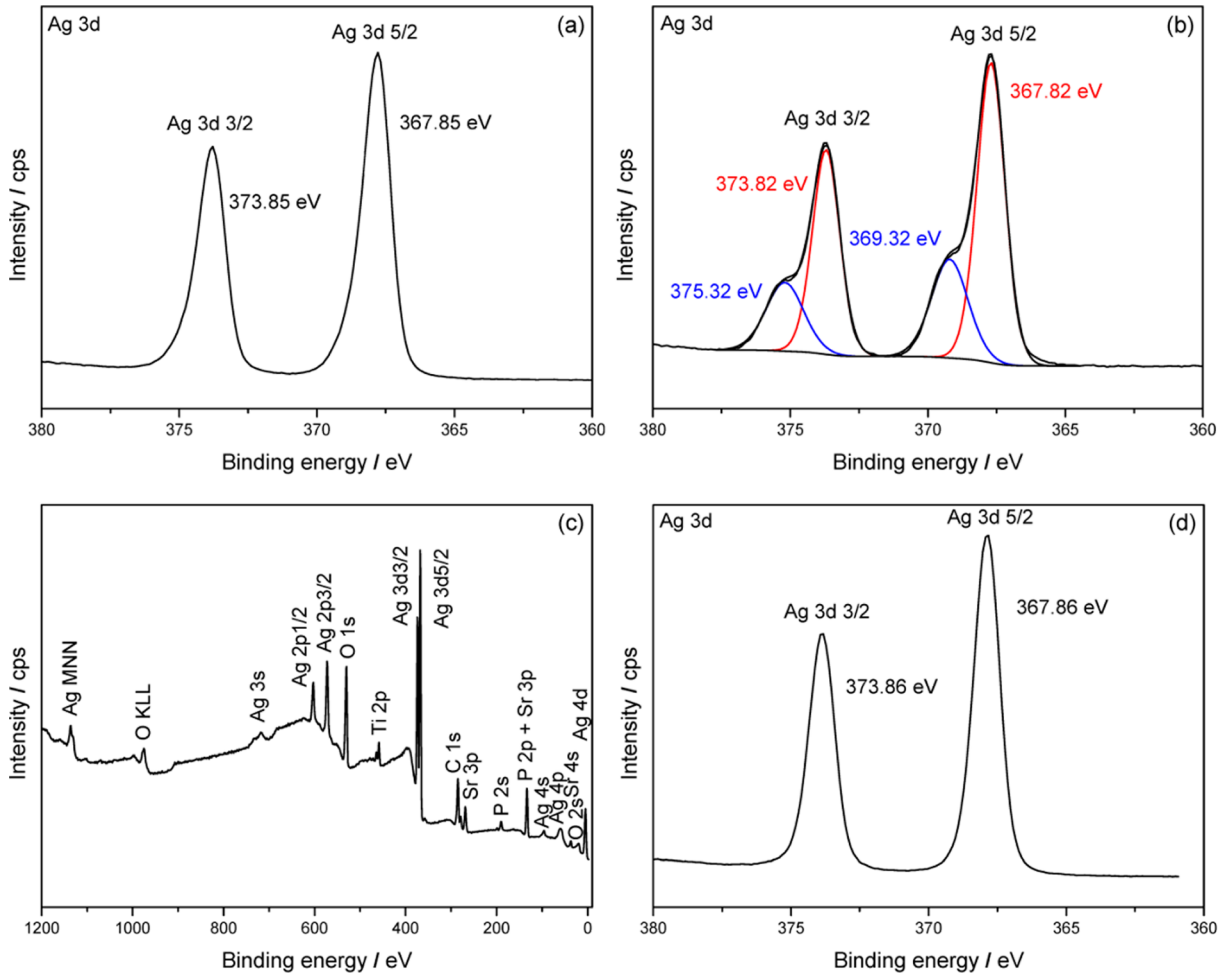

Figure 3. Typical XPS spectra of Ag 3d in Ag_3PO_4 (a), SA-1/20 (b), SA-1/20 without Ag (d), and wide scan spectra of SA-1/20 (c).

process. To confirm this deduction, $SrTiO_3$ was calcined at 800 °C to eliminate organic residuals, and the $SrTiO_3/Ag_3PO_4$ composite was further synthesized. XPS spectra of Ag 3d in Figure 3d demonstrates that metal Ag^0 species was thus avoided.

Figure 4 depicted the UV−vis absorption spectra of as-prepared samples. As shown in Figure 4, $SrTiO_3$ performed a 380 nm absorption band-edge in the UV region, corresponding to a band gap energy of 3.24 eV, which agreed with the results previously reported.[45] Spectra of Ag_3PO_4 indicated that it absorbed sunlight with wavelengths less than 530 nm, corresponding to a band gap energy of 2.42 eV. Band gap energy was calculated by the K-M method (see Figure S2 in Supporting Information). As $SrTiO_3$ was introduced into Ag_3PO_4, light absorption less than 500 nm was slightly depressed, owing to the decreased relative content of Ag_3PO_4. It could be noticed that the absorption in the long-wavelength range was gradually elevated in samples of larger molar ratio, which was attributed to the existence of highly dispersed tiny Ag^0 species.[46]

A room-temperature photoluminescence (PL) emission spectrum was recorded in order to investigate the migration and separation efficiency of photogenerated charge carriers in the as-prepared samples. Comparison of PL emission spectra for pure Ag_3PO_4 and SA-1/20 is shown in Figure 5. As for pure Ag_3PO_4, a strong emission peak at 440 nm and a shoulder peak around 550 nm were observed. A similar PL spectrum was

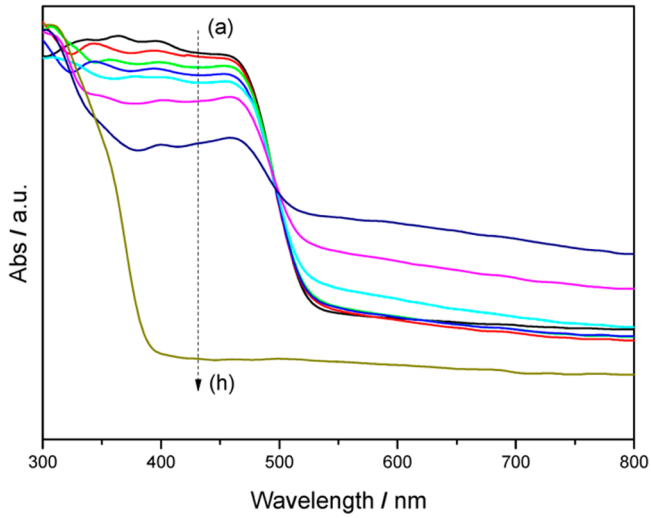

Figure 4. UV−vis spectra of $SrTiO_3/Ag_3PO_4$ composites with different molar ratios: (a) Ag_3PO_4, (b) SA-1/50, (c) SA-1/20, (d) SA-1/10, (e) SA-1/5, (f) SA-1/2, (g) SA-1/1, and (h) $SrTiO_3$.

obtained for SA-1/20, while the overall emission intensity was obviously reduced compared to that of pure Ag_3PO_4. Since PL emission is mainly due to the recombination of photogeneration electrons and holes, the weakened emission intensity in SA-1/20 thus indicates inhibition of recombination,

dx.doi.org/10.1021/cs5005079 | ACS Catal. 2014, 4, 3020−3026

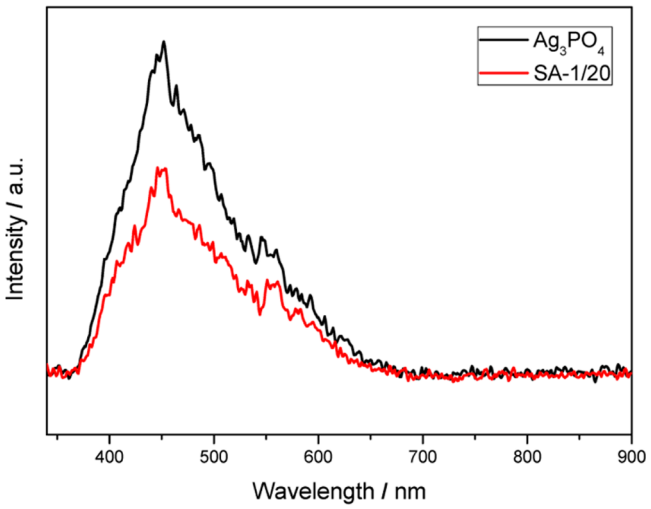

Figure 5. Photoluminescence spectra of as-prepared Ag_3PO_4 and SA-1/20 samples.

which lengthens the lifetime of charge carriers and is beneficial for the improvement of photocatalytic activity.[47,48]

3.2. Photocatalytic Activity. Photocatalytic activities of $SrTiO_3$, Ag_3PO_4, and $SrTiO_3/Ag_3PO_4$ composites were evaluated by O_2 evolution under visible-light irradiation (λ > 420 nm), and the results are shown in Figure 6. No O_2 was detected in the absence of either photocatalyst or light irradiation, eliminating water oxidation by photolysis of sacrificial solution or mechanocatalysis. A trace of O_2 was produced using pure phase $SrTiO_3$ catalyst, whereas the pure Ag_3PO_4 sample gave an excellent photocatalytic performance, with an initial rate of 967 μmol h^{-1} g_{cat}^{-1} and an A.Q.Y. of 12.4% at 420 nm. Introducing of $SrTiO_3$ resulted in a remarkable enhancement of O_2 evolution. As shown in Figure 6a,b, activity for O_2 production first increased and then gradually decreased with further loading of $SrTiO_3$. It is worth noting that initial rate and A.Q.Y. for photocatalytic O_2 evolution reached 1316 μmol h^{-1} g_{cat}^{-1} and 16.2%, respectively, with an optimal $SrTiO_3/Ag_3PO_4$ molar ratio of 1/20.

For comparison, photocatalytic activities of the physical mixtures with different molar ratios are shown in Figure 6c. The O_2 evolution was also enhanced but less efficiently, and the optimized molar ratio turned out to be 1/5. This is mainly ascribed to the poor contact and bad dispersion of $SrTiO_3$ on Ag_3PO_4 by simply physical mixing. These results indicate that loading of $SrTiO_3$ and contact between the two materials play a crucial role in the enhanced activity of Ag_3PO_4. Figure 6d showed the time course of O_2 evolution activity of SA-1/20 for 10 h. It could be recognized that the photocatalytic activity was linear at an early period and gradually decreased after irradiation for about 3 h. It should be noted that this phenomenon is not related to bad stability but is caused by the light shielding effect of photodeposited Ag particles, as has

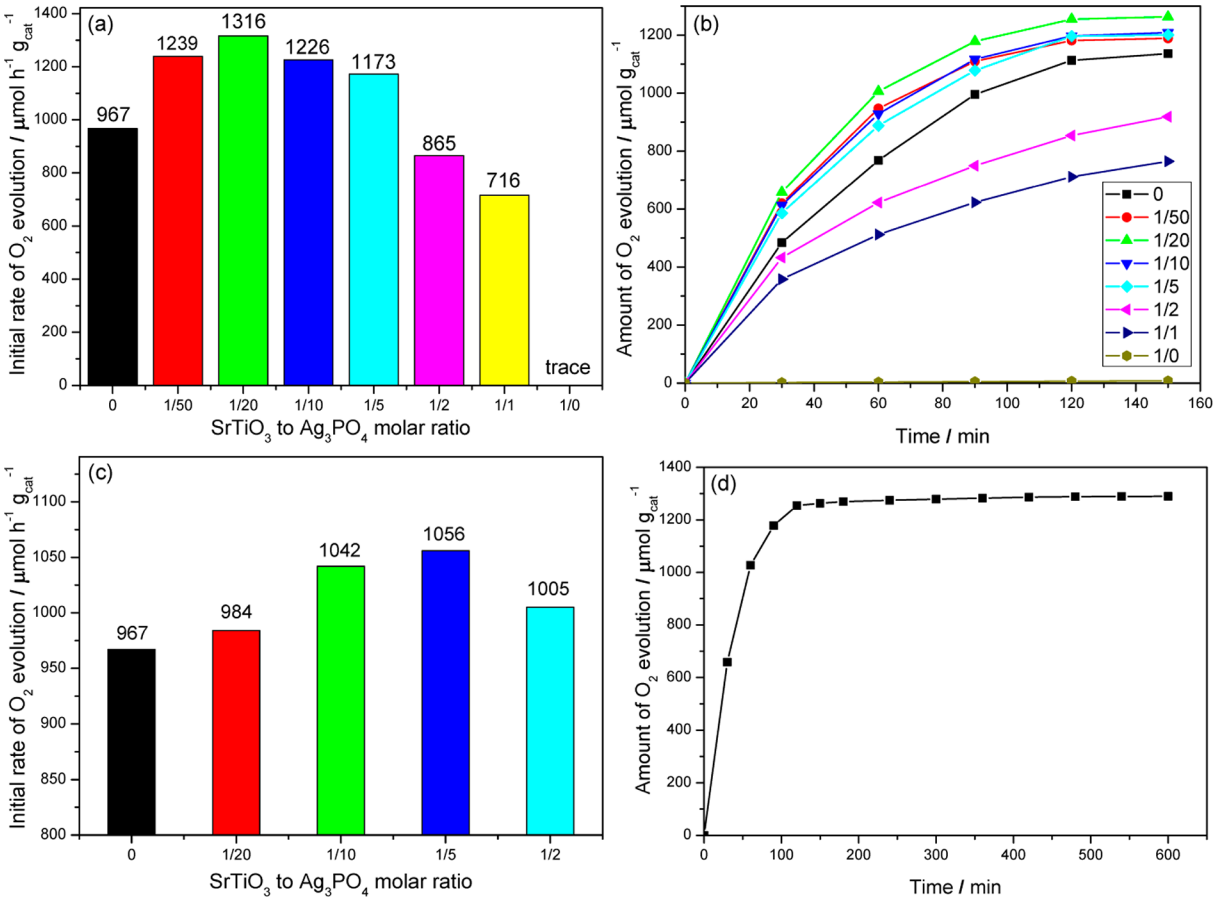

Figure 6. Photocatalytic activity for O_2 evolution of (a) $SrTiO_3/Ag_3PO_4$ composites with different molar ratios, (b) time course of $SrTiO_3/Ag_3PO_4$ composites with different molar ratios, (c) mixture of $SrTiO_3$ and Ag_3PO_4 with different molar ratios, and (d) SA-1/20 for 10 h, under visible-light irradiation (λ > 420 nm).

dx.doi.org/10.1021/cs5005079 | ACS Catal. 2014, 4, 3020−3026

been reported by pioneer studies.[8,15,17] Stable O_2 evolution from Fe^{3+} sacrificial solution also verified this point from another aspect (see Figure S3 in Supporting Information). The turnover number (T.O.N.) in terms of silver ions in the photocatalysts was calculated by evaluating the O_2 production for 12 h using 0.1 g of photocatalyst (see Figure S5 in Supporting Information). T.O.N. values of 1.08 and 1.41 were obtained for pure Ag_3PO_4 and SA-1/20 samples, respectively, meaning that this reaction is a photocatalytic process instead of a photochemical reaction. Herein, the T.O.N. was greatly underestimated because silver metal reduced from the sacrificial $AgNO_3$ would be deposited on the surface of the photocatalyst and prevent further water oxidation by blocking incident photon flux. Furthermore, XRD patterns of SA-1/20 were recorded both before and after the photocatalytic reaction and showed no significant change in composition except for the appearance of metal silver from photoreduction and deposition of sacrificial $AgNO_3$ (see Figure S6 in Supporting Information).

3.3. Mechanism of Enhanced O_2 Evolution. The enhancement of O_2 evolution for $SrTiO_3/Ag_3PO_4$ composites compared to pure Ag_3PO_4 photocatalyst could be ascribed to the following aspects: on the one hand, $SrTiO_3$ and Ag_3PO_4 possessed interlaced band structure. The band-edge potentials of CB and VB, designated as E_{CB} and E_{VB}, could be calculated from the following equation:

$$E_{VB} = \chi - E_0 + 1/2E_g$$

$$E_{CB} = \chi - E_0 - 1/2E_g$$

in which χ is the absolute electronegativity of the semiconductor, determined by the geometric mean of the absolute electronegativity of constituent atoms, which is defined as the arithmetic mean of the atomic electron affinity and the first ionization energy; E_0 is the energy of free electrons on the hydrogen scale; and E_g is the band gap of the semiconductor.[39,49,50] E_{CB} and E_{VB} of $SrTiO_3$ were determined to be −0.79 and 2.45 eV, while those of Ag_3PO_4 were 0.25 and 2.67 eV. On the basis of the alignment of their energy levels, an illustration of possible interface electron transfer behavior was proposed and shown in Figure 7. Ag_3PO_4 was first excited under visible-light irradiation. Since the loaded $SrTiO_3$ was in intimate contact with Ag_3PO_4, photoexcited holes from VBM of Ag_3PO_4 would be immigrated to the less positive VBM of $SrTiO_3$ and oxide H_2O to evolve O_2. The loaded $SrTiO_3$ provided additional active sites for the photocatalytic reaction. Meanwhile, the photoexcited electrons were transferred to the surface of Ag_3PO_4. It is known that metallic Ag^0 can serve as excellent acceptors and traps for photoexcited electrons; hence, the photoinduced electrons could be quickly transferred to Ag^0 species and consumed by the sacrificial Ag^+, as depicted in Figure 7.[15,36] This entire process would facilitate charge separation and indeed improved photocatalytic activity. Further investigation of O_2 evolution activity for the SA-1/20 sample without metal Ag showed only a slight decrease compared to that with Ag on the surface of Ag_3PO_4; hence it illustrates that it was $SrTiO_3$ rather than Ag that played the core role in the process (see Figure S4 in Supporting Information). In addition, pure $SrTiO_3$ was not active under visible-light irradiation, thus protecting Ag_3PO_4 from being reduced by photoexcited electrons of $SrTiO_3$.

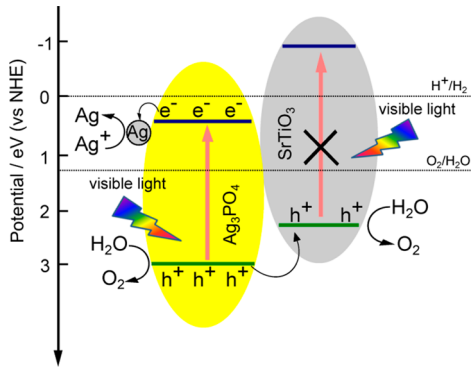

Figure 7. Schematic diagram of band structure and expected charge separation of $SrTiO_3/Ag_3PO_4$ composite under visible-light irradiation.

On the other hand, it has been widely reported that large surface area could greatly promote the photocatalytic reaction by offering more active sites.[51,52] The $SrTiO_3$ synthesized in this work possessed large surface area compared to that of the Ag_3PO_4 polyhedron due to its small particle size. As is claimed above, the loaded $SrTiO_3$ serves as a hole acceptor for photocatalytic water oxidation. Consequently, the larger surface area obtained from $SrTiO_3/Ag_3PO_4$ composites by introducing $SrTiO_3$ to Ag_3PO_4 gave rise to more active sites for water oxidation, which improved photocatalytic O_2 evolution.

The characterization results and mechanism proposed above imply that $SrTiO_3$ can serve as an efficient cocatalyst for photocatalytic water oxidation, which not only provides active sites for redox reaction but also inhibits recombination by promoting charge separation.

When more $SrTiO_3$ was loaded (molar ratio = 1/2, 1/1), visible-light absorption of $SrTiO_3/Ag_3PO_4$ composites were partly depressed. What's more, the assembling of $SrTiO_3$ particles resulted in less effective contact between two materials and meanwhile hindered the transference of both reactant and product. Therefore, activity of O_2 evolution decreased when the molar ratio of $SrTiO_3$ to Ag_3PO_4 was further increased.

4. CONCLUSIONS

An efficient photocatalyst for water oxidation was fabricated by loading a small amount of $SrTiO_3$ onto Ag_3PO_4 through a hydrothermal method. The as-synthesized $SrTiO_3/Ag_3PO_4$ composite showed improved photocatalytic activity compared to that of Ag_3PO_4, which was ascribed to the cocatalytic effect of $SrTiO_3$ providing both accelerated charge separation by band gap alignment and enriched active sites by enlarged surface area. This work offers useful guidance for developing an efficient O_2 producing photocatalyst and designing an overall photocatalytic water splitting system.

■ ASSOCIATED CONTENT

Supporting Information

FESEM images of $SrTiO_3/Ag_3PO_4$ composites with different molar ratios; Bandgap determination of Ag_3PO_4 and $SrTiO_3$ the by K-M method; photocatalytic O_2 evolution activity of SA-1/20 from Fe^{3+} sacrificial solution; comparison of photocatalytic O_2 evolution activity of samples with and without metal Ag species; T.O.N. measurement of pure Ag_3PO_4 and SA-1/20; XRD patterns of SA-1/20 before and after photocatalytic reaction; HRTEM images of as-prepared $SrTiO_3$; comparison of photocatalytic O_2 evolution activity of SA-1/20 with both TiO_2−Ag_3PO_4 composites and TiO_2; FESEM images of $SrTiO_3/Ag_3PO_4$ (SA-1/20) synthesized with different times of the second hydrothermal process; schematic formation

dx.doi.org/10.1021/cs5005079 | ACS Catal. 2014, 4, 3020−3026

mechanism of $SrTiO_3/Ag_3PO_4$; XRD pattern of the as-prepared sample when using the method of first Ag_3PO_4, then $SrTiO_3$; XPS etching profiles on SA-1/20; and EDS patterns and atomic content of consisting elements in SA-1/20. This material is available free of charge via the Internet at http://pubs.acs.org.

AUTHOR INFORMATION

Corresponding Author

*E-mail: lj-guo@mail.xjtu.edu.cn.

Notes

The authors declare no competing financial interest.

ACKNOWLEDGMENTS

This work was supported by National Natural Science Foundation of China (No. 51236007). We sincerely thank Jinwen Shi, Penghui Guo, and Xixi Wang for their help with analysis and discussions on the experiment.

REFERENCES

(1) Lewis, N. S. *Nature* **2001**, *414*, 589−590.
(2) Schloegl, R. *Nat. Mater.* **2008**, *7*, 772−774.
(3) Kudo, A.; Miseki, Y. *Chem. Soc. Rev.* **2009**, *38*, 253−278.
(4) Tong, H.; Ouyang, S. X.; Bi, Y. P.; Umezawa, N.; Oshikiri, M.; Ye, J. H. *Adv. Mater.* **2012**, *24*, 229−251.
(5) Shen, S. H.; Shi, J. W.; Guo, P. H.; Guo, L. J. *Int. J. Nanotechnol.* **2011**, *8*, 523−591.
(6) Chen, X. B.; Shen, S. H.; Guo, L. J.; Mao, S. S. *Chem. Rev.* **2010**, *110*, 6503−6570.
(7) Shi, J. W.; Guo, L. J. *Prog. Nat. Sci-Mater.* **2012**, *22*, 592−615.
(8) Shi, J. W.; Ye, J. H.; Li, Q. Y.; Zhou, Z. H.; Tong, H.; Xi, G. C.; Guo, L. J. *Chem.—Eur. J.* **2012**, *18*, 3157−3162.
(9) Liu, M. C.; Wang, L. Z.; Lu, G. Q.; Yao, X. D.; Guo, L. J. *Energy Environ. Sci.* **2011**, *4*, 1372−1378.
(10) Chen, Y. B.; Guo, L. J. *J. Mater. Chem.* **2012**, *22*, 7507−7514.
(11) Shen, S. H.; Zhao, L.; Zhou, Z. H.; Guo, L. J. *J. Phys. Chem. C* **2008**, *112*, 16148−16155.
(12) Zhang, K.; Guo, L. J. *Catal. Sci. Technol.* **2013**, *3*, 1672−1690.
(13) Liu, M. C.; Jing, D. W.; Zhou, Z. H.; Guo, L. J. *Nat. Commun.* **2013**, *4*, 2278−2285.
(14) Tang, J. W.; Durrant, J. R.; Klug, D. R. *J. Am. Chem. Soc.* **2008**, *130*, 13885−13891.
(15) Yi, Z. G.; Ye, J. H.; Kikugawa, N.; Kako, T.; Ouyang, S. X.; Stuart-Williams, H.; Yang, H.; Cao, J. Y.; Luo, W. J.; Li, Z. S.; Liu, Y.; Withers, R. L. *Nat. Mater.* **2010**, *9*, 559−564.
(16) Umezawa, N.; Ouyang, S. X.; Ye, J. H. *Phys. Rev. B* **2011**, *83*, 035202(1−8).
(17) Martin, D. J.; Umezawa, N.; Chen, X. W.; Ye, J. H.; Tang, J. W. *Energy Environ. Sci.* **2013**, *6*, 3380−3386.
(18) Guan, X. J.; Shi, J. W.; Guo, L. J. *Int. J. Hydrogen Energy* **2013**, *38*, 11870−11877.
(19) Wang, Y. J.; Wang, Q. S.; Zhan, X. Y.; Wang, F. M.; Safdar, M.; He, J. *Nanoscale* **2013**, *5*, 8326−8339.
(20) Zhang, H. C.; Huang, H.; Ming, H.; Li, H. T.; Zhang, L. L.; Liu, Y.; Kang, Z. H. *J. Mater. Chem.* **2012**, *22*, 10501−10506.
(21) Yao, W. F.; Zhang, B.; Huang, C. P.; Ma, C.; Song, X. L.; Xu, Q. J. *J. Mater. Chem.* **2012**, *22*, 4050−4055.
(22) Yang, X. F.; Cui, H. Y.; Li, Y.; Qin, J. L.; Zhang, R. X.; Tang, H. *ACS Catal.* **2013**, *3*, 363−369.
(23) Chen, G. D.; Sun, M.; Wei, Q.; Zhang, Y. F.; Zhu, B. C.; Du, B. *J. Hazard Mater.* **2013**, *244*, 86−93.
(24) Cui, H. Y.; Yang, X. F.; Gao, Q. X.; Liu, H.; Li, Y.; Tang, H.; Zhang, R. X.; Qin, J. L.; Yan, X. H. *Mater. Lett.* **2013**, *93*, 28−31.
(25) Dong, P. Y.; Wang, Y. H.; Cao, B. C.; Xin, S. Y.; Guo, L. N.; Zhang, J.; Li, F. H. *Appl. Catal., B* **2013**, *132*, 45−53.
(26) Jiang, B. J.; Wang, Y. H.; Wang, J. Q.; Tian, C. G.; Li, W. J.; Feng, Q. M.; Pan, Q. J.; Fu, H. G. *ChemCatChem* **2013**, *5*, 1359−1367.
(27) Yang, X. F.; Qin, J. L.; Jiang, Y.; Li, R.; Li, Y.; Tang, H. *RSC Adv.* **2014**, *4*, 18627−18636.
(28) Zhai, W. Y.; Li, G. P.; Yu, P.; Yang, L. F.; Mao, L. Q. *J. Phys. Chem. C* **2013**, *117*, 15183−15191.
(29) Kumar, S.; Surendar, T.; Baruah, A.; Shanker, V. *J. Mater. Chem. A* **2013**, *1*, 5333−5340.
(30) Hou, Y.; Zuo, F.; Ma, Q.; Wang, C.; Bartels, L.; Feng, P. Y. *J. Phys. Chem. C* **2012**, *116*, 20132−20139.
(31) Konta, R.; Ishii, T.; Kato, H.; Kudo, A. *J. Phys. Chem. B* **2004**, *108*, 8992−8995.
(32) Hara, S.; Yoshimizu, M.; Tanigawa, S.; Ni, L.; Ohtani, B.; Irie, H. *J. Phys. Chem. C* **2012**, *116*, 17458−17463.
(33) Townsend, T. K.; Browning, N. D.; Osterloh, F. E. *Energy Environ. Sci.* **2012**, *5*, 9543−9550.
(34) Niishiro, R.; Tanaka, S.; Kudo, A. *Appl. Catal., B* **2014**, *150*, 187−196.
(35) Hara, S.; Irie, H. *Appl. Catal., B* **2012**, *115*, 330−335.
(36) Guo, J. J.; Ouyang, S. X.; Li, P.; Zhang, Y. J.; Kako, T.; Ye, J. H. *Appl. Catal., B* **2013**, *134−135*, 286−292.
(37) Zhang, N.; Shi, J. W.; Mao, S. S.; Guo, L. J. *Chem. Commun.* **2014**, *50*, 2002−2005.
(38) Štengl, V.; Popelková, D.; Vláčil, P. *J. Phys. Chem. C* **2011**, *115*, 25209−25218.
(39) Li, C. J.; Zhang, P.; Lv, R.; Lu, J. W.; Wang, T.; Wang, S. P.; Wang, H. F.; Gong, J. L. *Small* **2013**, *9*, 3951−3956.
(40) Kuang, Q.; Yang, S. H. *ACS Appl. Mater. Interfaces* **2013**, *5*, 3683−3690.
(41) Shi, J. W.; Ye, J. H.; Ma, L. J.; Ouyang, S. X.; Jing, D. W.; Guo, L. J. *Chem.—Eur. J.* **2012**, *18*, 7543−7551.
(42) Shi, J. Y.; Liu, G. J.; Wang, N.; Li, C. J. *Mater. Chem.* **2012**, *22*, 18808−18813.
(43) Wang, D. F.; Kako, T.; Ye, J. H. *J. Am. Chem. Soc.* **2008**, *130*, 2724−2725.
(44) Wang, W. S.; Du, H.; Wang, R. X.; Wen, T.; Xu, A. W. *Nanoscale* **2013**, *5*, 3315−3321.
(45) Wang, D. F.; Ye, J. H.; Kako, T.; Kimura, T. *J. Phys. Chem. B* **2006**, *110*, 15824−15830.
(46) Bi, Y. P.; Hu, H. Y.; Ouyang, S. X.; Jiao, Z. B.; Lu, G. X.; Ye, J. H. *Chem.—Eur. J.* **2012**, *18*, 14272−14275.
(47) Peng, T. Y.; Li, K.; Zeng, P.; Zhang, Q. G.; Zhang, X. G. *J. Phys. Chem. C* **2012**, *116*, 22720−22726.
(48) Ge, L.; Han, C. C. *Appl. Catal., B* **2012**, *117*, 268−274.
(49) Huang, J. D.; Liu, J. Y.; Han, K. L. *Int. J. Hydrogen Energy* **2012**, *37*, 17870−17881.
(50) Xu, H.; Xu, Y. G.; Li, H. M.; Xia, J. X.; Xiong, J.; Yin, S.; Huang, C. J.; Wan, H. L. *Dalton Trans.* **2012**, *41*, 3387−3394.
(51) Yu, H.; Ouyang, S. X.; Yan, S. C.; Li, Z. S.; Yu, T.; Zou, Z. G. *J. Mater. Chem.* **2011**, *21*, 11347−11351.
(52) Liang, Q. H.; Ma, W. J.; Shi, Y.; Li, Z.; Yang, X. M. *CrystEngComm* **2012**, *14*, 2966−2973.